# *MICROMACHINED STIMULATING ELECTRODES*

**Quarterly Report #9**

(Contract NIH-NINDS-N01-NS-2-2379)

October --- December 1994

Submitted to the

**Neural Prosthesis Program**
National Institute of Neurological Disorders and Stroke
National Institutes of Health

by the

Solid-State Electronics Laboratory
Bioelectrical Sciences Laboratory
Department of Electrical Engineering and Computer Science
University of Michigan
Ann Arbor, Michigan
48109-2122

February 1995

# *MICROMACHINED STIMULATING ELECTRODES*

## ***Summary***

During the past quarter, research under this program has focused in several areas. We have continued to produce a variety of passive stimulating probes and provide them to internal and external users. Probes have now been fabricated using procedures reported in the last report (RTA after iridium deposition, buffered HF etch after RIE, and complete sample drying prior to sputtering) to improve iridium adhesion. Using 500Å of titanium under 3000Å of iridium with these procedures, no adhesion problems have been observed. In addition, the interfacial barrier to current flow frequently observed in the past on metal-polysilicon contacts (electrode sites) are no longer present. We have also redefined our site formation procedure to allow thorough cleaning of the sites after RIE and before metal deposition. The new procedure uses an additional mask so that the dielectric etch and metal deposition are separate steps. Probes are now in process using this new structure. Work is also proceeding to complete the development of new site activation and characterization facilities. In addition, we are continuing modeling activities to understand current flow around implanted stimulating sites and are analyzing the material seen on stimulating sites that have been used chronically in tissue using XPS.

Active probes have now been tested successfully with the external computer interface developed for them. In addition, tests are being conducted to better understand electrode site performance when used with STIM-2. An unexpected leakage current between the sites and the negative supply rail has been noted on at least some of the STIM-2 chips. The amplitude of this current is approximately 25nA. While small, it appears that this current can polarize small electrode sites sufficiently to drag them down near the edge of the water window so that active cathodic-first stimulation would exceed the window. While studies of these phenomena are continuing, it appears that it will be necessary to tie electrodes to a known potential between pulses. This can be done with the circuitry built into STIM-2 and is in line with recent studies by other investigators that indicate such anodic bias is helpful in terms of chronic impedance and charge delivery.

Terry - the answer to your question at the site visit!

# *MICROMACHINED STIMULATING ELECTRODES*

## *1. Introduction*

The goal of this research is the development of active multichannel arrays of stimulating electrodes suitable for studies of neural information processing at the cellular level and for a variety of closed-loop neural prostheses. The probes should be able to enter neural tissue with minimal disturbance to the neural networks there and deliver highly-controlled (spatially and temporally) charge waveforms to the tissue on a chronic basis. The probes consist of several thin-film conductors supported on a micromachined silicon substrate and insulated from it and from the surrounding electrolyte by silicon dioxide and silicon nitride dielectric films. The stimulating sites are activated iridium, defined photolithographically using a lift-off process. Passive probes having a variety of site sizes and shank configurations have been fabricated successfully and distributed to a number of research organizations nationally for evaluation in many different research preparations. For chronic use, the biggest problem associated with these passive probes concerns their leads, which must interface the probe to the outside world. Even using silicon-substrate ribbon cables, the number of allowable interconnects is necessarily limited, and yet a great many stimulating sites are ultimately desirable in order to achieve high spatial localization of the stimulus currents.

The integration of signal processing electronics on the rear of the probe substrate (creating an "active" probe) allows the use of serial digital input data which can be demultiplexed on the probe to provide access to a large number of stimulating sites. Our goal in this area of the program has been to develop a family of active probes capable of chronic implantation in tissue. For such probes, the digital input data must be translated on the probe into per-channel current amplitudes which are then applied to the tissue through the sites. Such probes require five external leads, virtually independent of the number of sites used. As discussed in our previous reports, we are now developing a series of three active probes containing CMOS signal processing electronics. Two of these probes are slightly redesigned versions of an earlier first-generation set of designs and are designated as STIM-1A and STIM-1B. The third probe, STIM-2, is a second-generation version of our high-end first-generation design, STIM-1. All three probes provide 8-bit resolution in setting the per-channel current amplitudes. STIM-1A and -1B offer a biphasic range using ±5V supplies from 0μA to ±254μA with a resolution of 2μA, while STIM-2 has a range from 0 to ±127μA with a resolution of 1μA. STIM-2 offers the ability to select 8 of 64 electrode sites and to drive these sites independently and in parallel, while -1A allows only 2 of 16 sites to be active at a time (bipolar operation). STIM-1B is a monopolar probe, which allows the user to guide an externally-provided current to any one of 16 sites as selected by the digital input address. The high-end STIM-2 contains provisions for numerous safety checks and for features such as remote impedance testing in addition to its normal operating modes. It also offers the option of being able to record from any one of the selected sites in addition to stimulation.

During the past quarter, research on this contract has focused in several areas. We have fabricated passive probes using the techniques noted in the last report and defined by the studies of iridium adhesion reported there. The probes have shown no adhesion problems and none of the electrical conduction barriers that were often seen in the past. We have also modified the procedure for site formation used in the past to allow a vigorous cleaning step between contact formation and site metal deposition. Probes are now being fabricated with this new procedure. We have also continued our modeling of current flow around stimulating sites and analysis of the material seen on sites used for

chronic stimulation in-vivo. Work on the development of an automated station for iridium activation and characterization is nearing completion, and in-vitro characterization of active stimulating probes is underway. Electrode potential recovery times were explored during the past term driving both discrete capacitors and activated electrode sites. The results in each of these areas are described below.

## 2. *Modified Site Formation Techniques*

As mentioned in the previous quarterly progress report, during the past few years we have had increasing difficulty in achieving good metal adhesion in the fabrication of iridium electrode sites; more recently, similar problems have been encountered with the adhesion of gold bonding pads on the probes. In spite of investigations into metal sputtering conditions and other process parameters, the problem continued to worsen over the past three years. Due to the compressive stress as deposited, the iridium tended to simply buckle or pop off of the substrate, leaving bubbles of local lifting in the metallization or exposing the substrate completely. This problem has been accompanied by an electrical conductance barrier which appeared to be present at many of our contacts. This barrier was evident as a higher-than-normal impedance between the interconnect material and the site metal that could be broken down by passing current through the site at voltages of from a few volts to tens of volts. These problems have seriously reduced the yield of recently fabricated probes.

A detailed study (discussed in depth in the previous quarterly progress report) of this problem led to an understanding of what was happening; the "barrier film" and the adhesion problem were really two manifestations of the same problem and were due to the formation of a fluorocarbon film on the polysilicon interconnect during the RIE opening of the probe dielectrics to define the electrode sites. The fluorocarbon film, polytetrafluoroethylene (commonly known as Teflon), has a high resistivity and is commonly used as an *anti*-sticking layer. The formation of the fluorocarbon film is enhanced by overetching into the polysilicon interconnect, which was a standard procedure in order to be sure of complete removal of the dielectric layers from the contacts/site areas. It was also found that residual moisture in contacts due to incomplete drying prior to metal deposition was a second factor reducing metal adhesion.

As discussed in the last report, new measures have been taken to solve these iridium adhesion problems. During the last quarter, we have had several runs come out of the lab, including probes from the masks EMORY, HMRI, and HI-DENS. Although none of these wafers were processed using the complete new site formation technique described below, the other steps outlined in the last report were taken to ensure adequate site adhesion (RTA after iridium deposition, buffered HF etch after RIE, and complete sample drying prior to sputtering). Probes from each of these runs were probed both before and after the final EDP etch, and the current-voltage characteristics observed were very linear, indicating that there was no barrier between the titanium and the polysilicon. Sites on probes from each run were also optically inspected using scanning electron microscopy. As shown in the photos in Fig. 1, none of the bubbling or peeling seen in previous runs is evident in these new probes. AC impedance tests at 1kHz also indicate that the site impedances are consistent and within the range expected for a specific site size.

As a result of these studies, several changes have been made to the site/pad formation process flow in order to improve the metal adhesion. An extra masking layer was added to permit an etching/cleaning step after the RIE etch and before the actual

deposition of the metal into the opened site area. An extra drying step was added prior to metal deposition. An RTA annealing step was added as a standard step following lift-off of the Ti/Ir in order to promote good adhesion and reduce the site impedance. The new step-by-step site/pad formation process flow is summarized below in Table 1. Several significant points will be discussed in more depth next in relation to their importance in the realization of good properly functioning electrode sites and bonding pads.

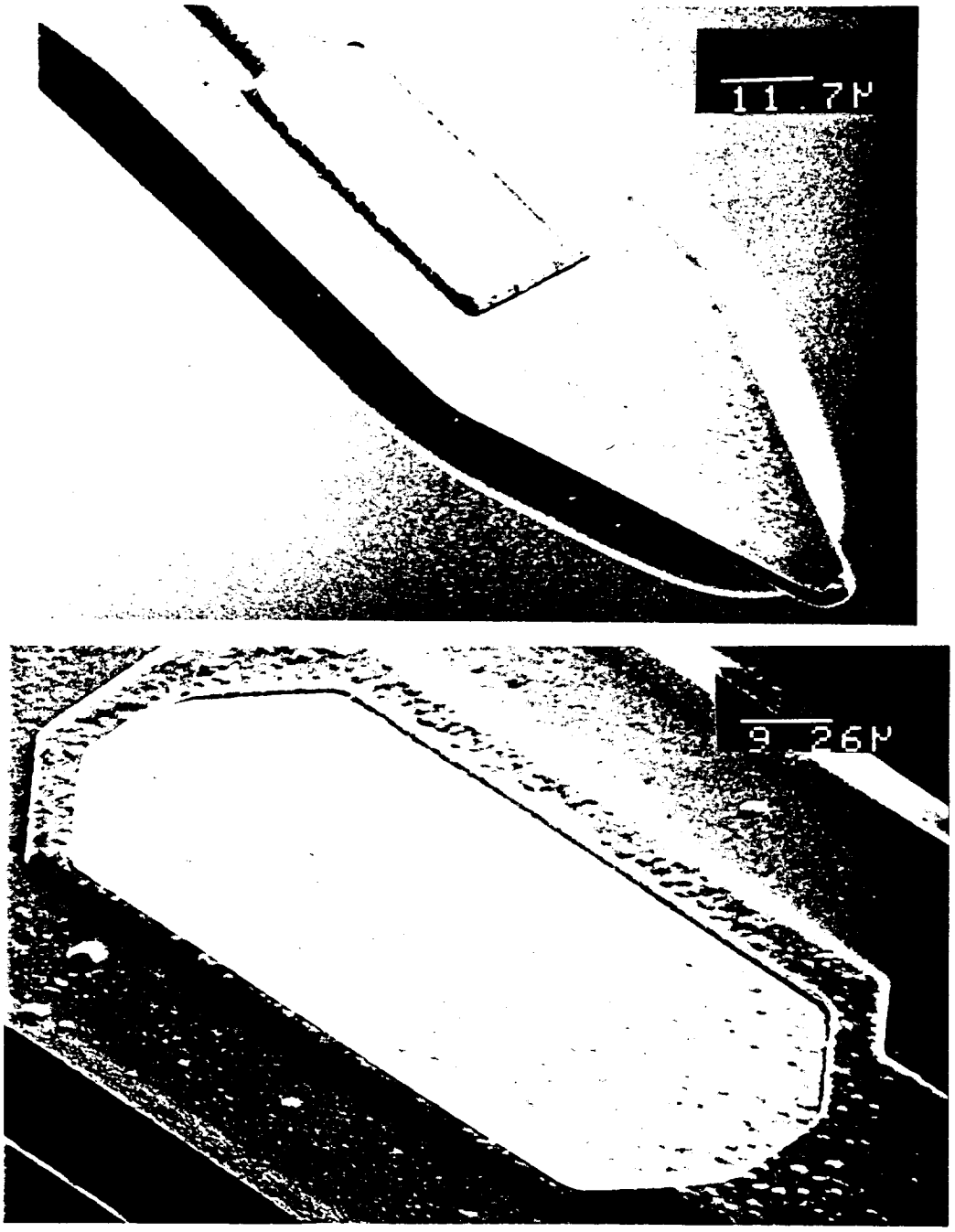


Fig. 1: SEM photographs of iridium sites on finished probes fabricated recently using the revised processing sequence. The probes show no adhesion problems, nor do they show any of the barrier potentials that were common on earlier fabrication runs. The top photo is of a site on a SCHMIDT-type probe (13μm x 38μm), and the bottom on a SX07-type probe (26μm x 74μm).

| **Mask 4: (All Site Contacts)** |
|---|
| • Normal lithography |
| **RIE etch contacts** |
| • Stop etch with 500-1000 angstroms oxide remaining in bottom of contact * |
| **Strip photoresist/clean contacts** |
| • Strip: $H_2SO_4$:$H_2O_2$ 1.2:1, 10 min. * |
| • Rinse: DI-$H_2O$, 3 min.; spin dry |
| **Mask 5: (Iridium Site Metal)** |
| • Normal lithography |
| **Wet etch contacts** |
| • Etch: BHF, 1.0 min. * |
| • Rinse: DI-$H_2O$, 2 min.; spin dry |
| • Drybake: 5 min. @ 110 °C; (immediately load into sputterer) * |
| **Sputter Iridium** |
| **Liftoff** |
| **Anneal** |
| • RTA, 500 °C, Argon, 30 sec. |
| **Mask 6: (Gold Pad Metal)** |
| • Normal lithography |
| **Wet etch contacts** |
| • Etch: BHF, 1.0 min. * |
| • Rinse: DI-$H_2O$, 2 min.; spin-dry |
| • Drybake: 5 min. @ 110 °C; (immediately load into sputterer) |
| **Sputter Gold** |
| **Liftoff** |

* New or altered steps.

Table 1: Site/pad fabrication process flow.

The original site structure used for the probes is shown below in Fig. 2. This site structure is attractive in that it only requires one mask and the metal is self-aligned to the contact opening. The difficulty is in the fact that the process does not allow for thorough cleaning of the contact opening between the dry etch (RIE) and the metal deposition because of the necessity of maintaining the integrity of the photoresist for the liftoff metal definition step. It was standard to perform a 30 second buffered HF dip in an attempt to ensure that all of the oxide was cleared from the contact area. However, the buffered HF does not etch Teflon; therefore, it remains behind as an interfacial layer. As mentioned in the previous quarterly report, the Teflon layer appears to become an even more significant problem if the contact is intentionally overetched (in the RIE). The height of the metal coverage along the dielectric sidewall can vary, but there is a thin area in the corner of the contact as shown.

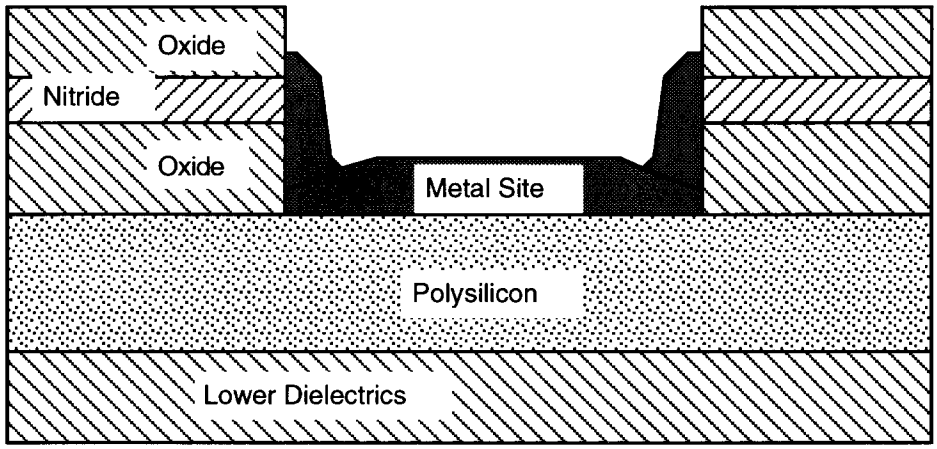


Fig. 2: One half of the original self-aligned site/pad structure used with the probes.

The new pad/site structure is realized by simultaneously defining the contact areas of both the sites and the pads and performing an anisotropic dry etch (RIE) through the upper dielectric layers (Fig. 3) to stop just short of the polysilicon surface, leaving approximately 500-1000Å of oxide in the bottom of the contact opening. The photoresist is then stripped and the are wafers cleaned in $H_2SO_4$:$H_2O_2$. Next, the wafers are patterned for the Ir sites, which are defined to overlap the upper oxide layer. The thin oxide layer in the site contact is etched away isotropically in buffered HF, down to the underlying polysilicon (Fig. 4). This is a critical step in that the amount lateral etch of the bottom oxide layer must be kept to a minimum in order to ensure a good seal between the site metal and the oxide in the site corner so that the subsequent etch in EDP does not attack the polysilicon interconnect. If there is any Teflon in the bottom of the contact opening, the buffered HF will undercut the oxide, thereby removing it.

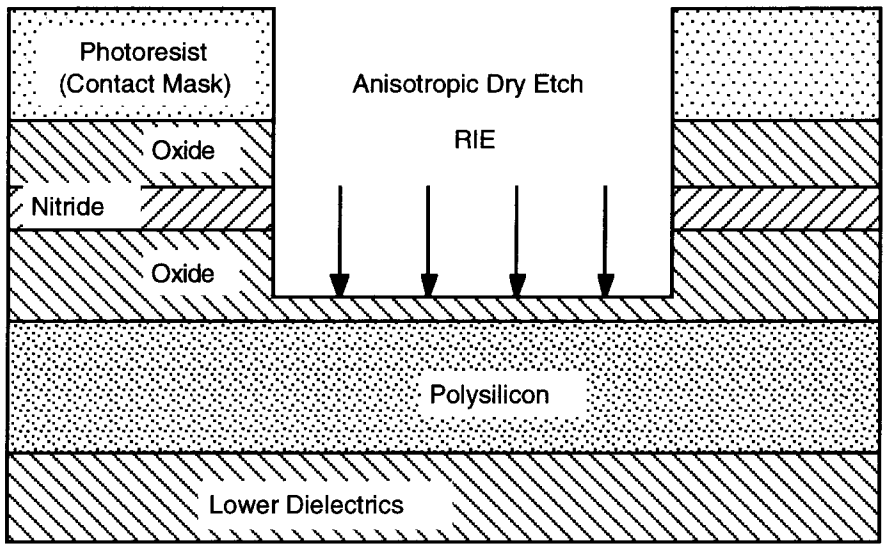


Fig. 3: As the first step in realizing the new site/pad structure, an anisotropic dry etch (RIE) is used with the site/contact mask to etch down into the lower oxide layer.

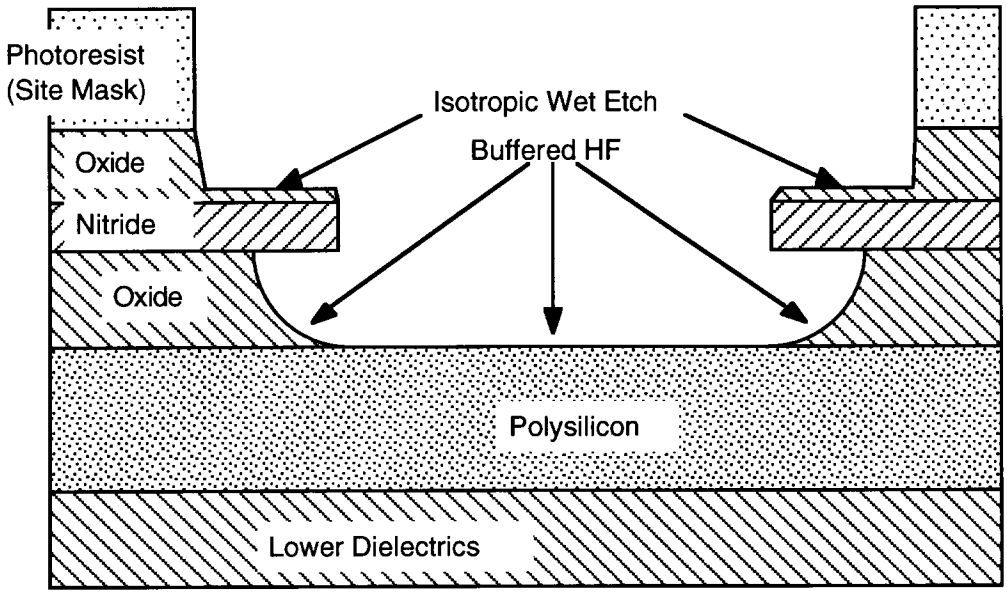


Fig. 4: As the second step in realizing the new site/pad structure, an isotropic wet etch (buffered HF) is used with the site or pad mask to open the underlying polysilicon.

During the HF etch of the lower oxide layer during the site opening, it will undercut the silicon nitride layer slightly, causing a *cave* to form under the nitride as shown in Fig. 5. As long as this is relatively shallow, the metal will seal around it, resulting in a metal ring around the edge of the sight over the nitride. This can still be slightly recessed below the field oxide surface as shown in Fig. 5. However, if the cave depth becomes excessive, the metal will not seal and a small edge of exposed polysilicon will be left which will be attacked in EDP, destroying the probe. Since the thickness of our metal is now 3500Å (500Å Ti plus 3000Å Ir), this should not be a significant problem. The final semi-recessed metal site/pad structure is as shown. The actual size of the dielectric *cave* is determined by the amount of time in buffered HF. The undercut must be reduced to ensure proper protection of the underlying polysilicon. Experiments with varying HF etch times indicate that etch times in excess of about one minute will result in excessive etch-back of the bottom oxide and therefore failure to provide protection for the polysilicon against the EDP etch. If the metal is thin or the lower oxide is thick, the metal ring around the edge of the site will be electrically isolated from the site; however, for thicker metal it will be connected.

The new overall pad/site structure is shown in Fig. 6, which is an iridium recording site on a probe that has undergone the final EDP etch. This demonstrates that the metal (Ti/Ir) overlaps the LPCVD dielectric over the polysilicon pad. A benefit of this configuration is that larger site areas (e.g., on stimulating probes) can be realized without an increase in the size of the underlying polysilicon interconnects; therefore, there is no loss of lead density on the probe shanks. Figure 7 shows the cross-section of the outer rim of a gold bonding pad. The pad was broken in the middle and then dipped in HF-Nitric acid in order to etch the polysilicon and oxide layers back selectively, lending more clarity to the various layers of the pad. Polysilicon is etched very rapidly in

HF-Nitric, causing the hollow channel observed in the center. A diagram of the same pad rim is included in Fig. 8 to help define the different layering. This picture demonstrates a slight seam on the inside edge of the pad rim at the lower edge of the nitride due to the lateral etch-back of the lower LPCVD oxide layer under the LPCVD nitride. This is confirmed in the close-up view shown in Fig. 9. It is also clear, however, that the metal (Cr/Au) extends up the side of the lower oxide layer forming a protective seal over the poly against the final EDP etch. This seal was confirmed by the fact that the polysilicon had survived the EDP etch.

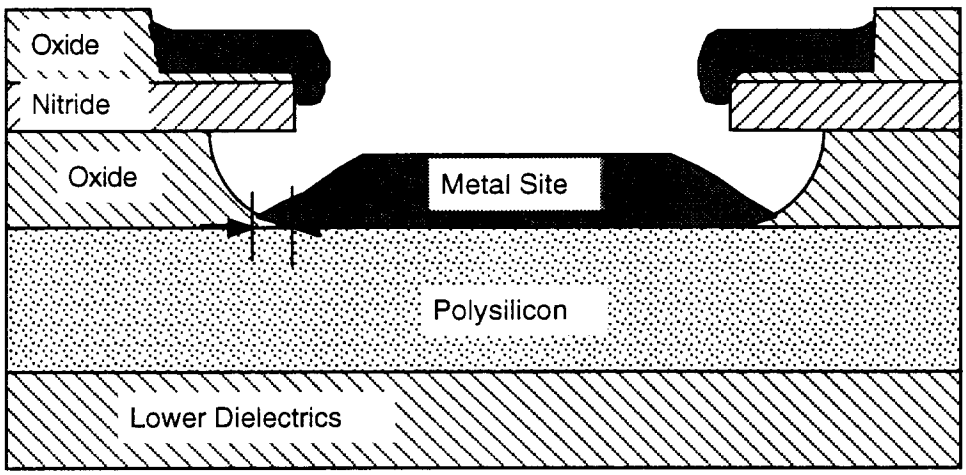


Fig. 5: The new semi-recessed site/pad structure. The metal ring overlapping the field oxide may or may not be electrically connected depending on the oxide and metal thicknesses used. The final oxide etch time must be limited to restrict the lateral undercut under the nitride so as not to expose the polysilicon to the final EDP probe separation etch.

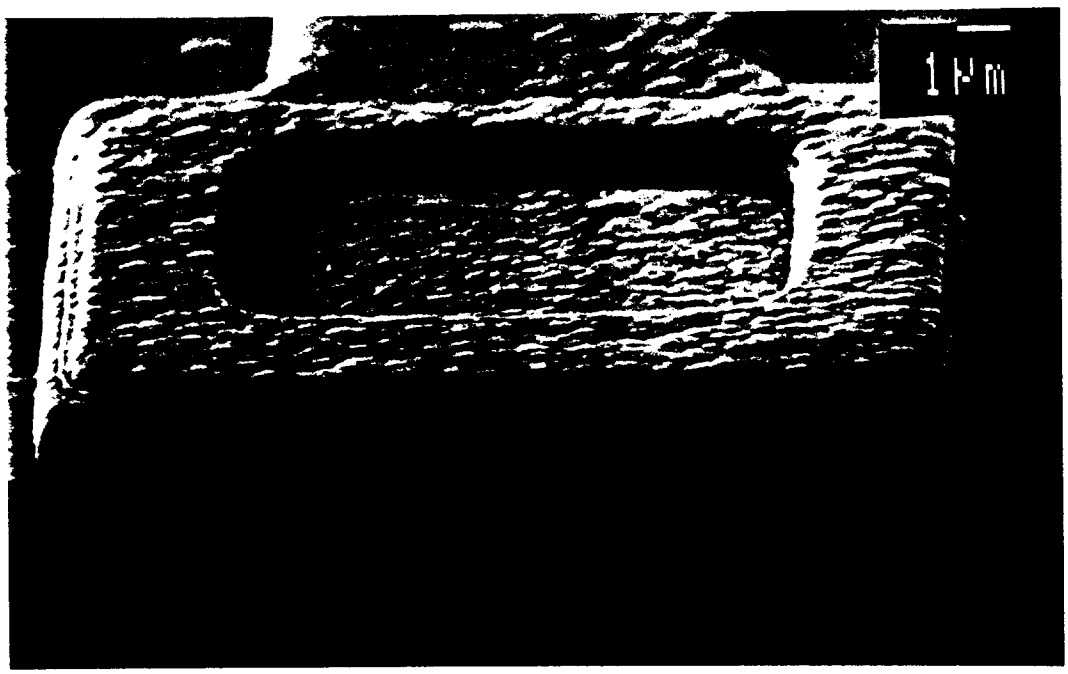


Fig. 6: An iridium recording site on a completed probe which demonstrates the overall profile of the new site/pad structure.

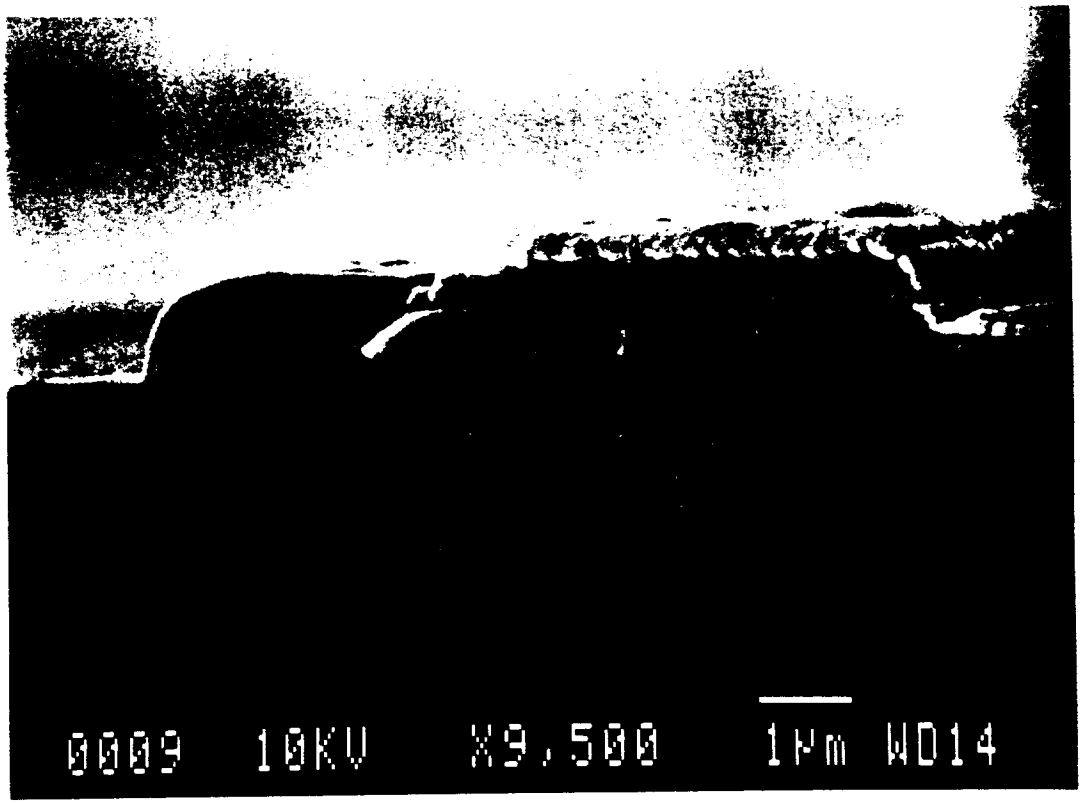


Fig. 7: The cross-section of the outer rim of a gold bonding pad. The oxide lateral etch effect is observable as the seam visible in the metal sidewall.

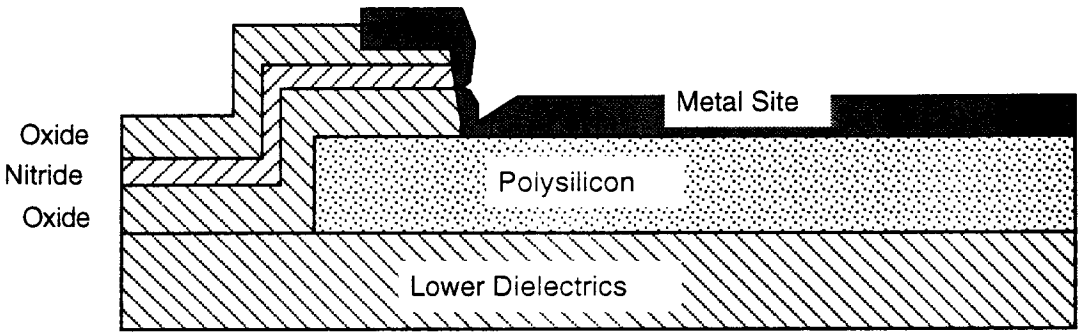


Fig. 8: A diagram of the cross-section of the outer rim of a gold bonding pad (as shown in Fig. 7).

The metal seam does not appear to be a problem if good etch control is realized. In order to make the etch control less critical, the thickness of the bottom LPCVD oxide thickness will be reduced from 3000 to 2000Å in future probe runs. In order to maintain a neutral stress in the upper dielectric layer, the upper LPCVD oxide layer will be increased from 3000 to 4000Å. Reduction of the thickness of the lower oxide layer is expected to reduce the size of the seam, possibly allowing for its complete elimination.

The final metal thickness (4000Å) now approaches that of the complete lower oxide layer (including both a thermal oxide and the deposited LPCVD) increasing the likelihood of completely covering the opening of the bottom oxide *cave*. The lower oxide thickness cannot be reduced below 2000Å without starting to have a significant effect on the stress of the layer. At thicknesses lower than about 2000Å, the stress begins to drop off sharply which would have the effect of disrupting the stress balance in the triple dielectric layering.

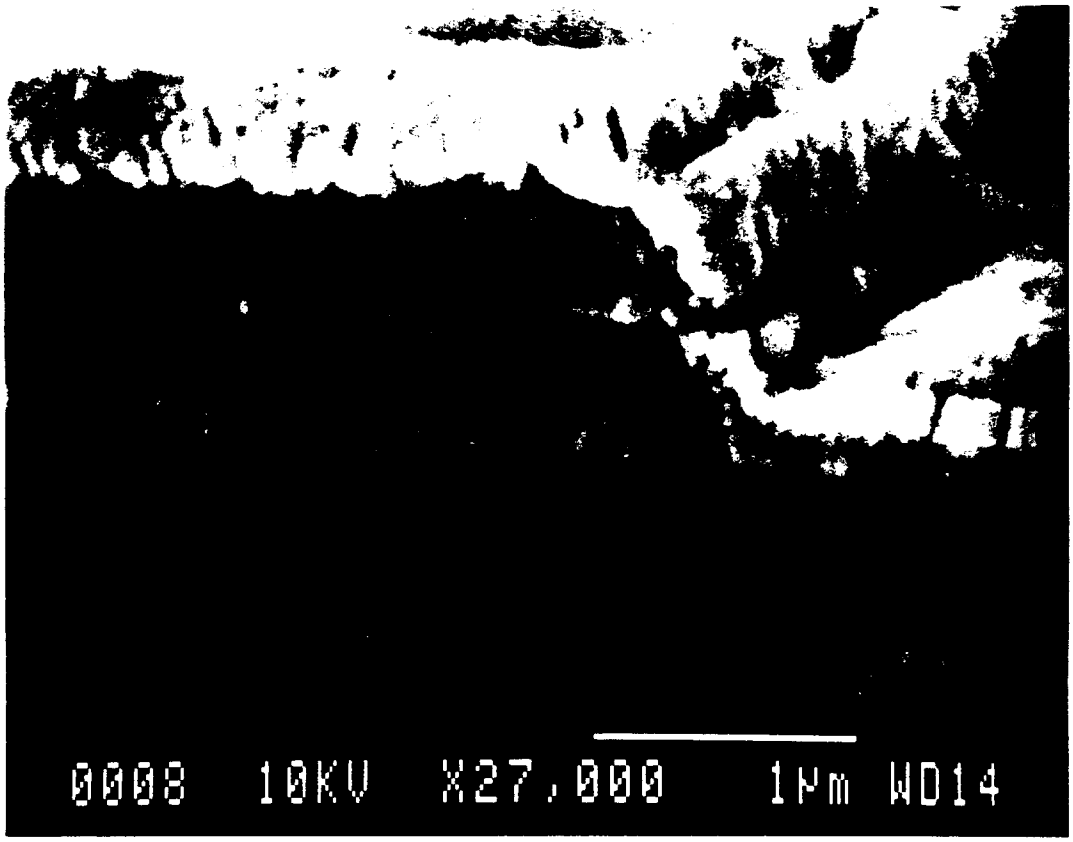


Fig. 9: A close-up view of the pad sidewall, confirming that the position of the seam at the lower edge of the nitride layer and well above the polysilicon.

During the coming term, we will fabricate probes with this new site structure so that the performance of such sites can be reported. We anticipate no further problems with iridium site adhesion or the barrier problems that plagued past runs.

## *3. In-Vivo Current Flow and Impedance Studies*

*Iridium Site Characterization*

During the past quarter, results were obtained in several areas. Finite element software was used to generate models of current flow around probe shanks. Further analysis was performed on an electrode site retrieved from a chronic implant. Finally, updates were made to the chronic stimulation instrumentation to allow more experimental flexibility.

*Current Flow Modeling*

The finite element method was used to generate approximate solutions to differential equations that are analytically intractable. We are currently using the finite element program COSMOS/EM (Structural Research). COSMOS/EM is designed to solve three-dimensional electromagnetic problems, such as Laplace's equation

$$\nabla^2 \phi = 0$$

(where $\phi$ is electrical potential) for current flow through a conducting media or electric field strength in a dielectric. Before the problem is solved, several conditions must be established. First, the geometry must be defined. In the case of a monopolar stimulating electrode, that geometry is a disk held at a known potential with respect to an infinite ground. The bipolar case is a little more complex since it involves two coplanar disks of opposite potential. However, in the latter case a symmetric model is used, taking advantage of the zero potential plane halfway between the two disks. Therefore, only one-half of the model needs to be solved. The disks are placed on nonconducting shanks and the disk and shank are surrounded by conducting media. Next, the nature of the media needs to be defined. The directional conductivities and the permittivity of the material are the parameters of interest. The conductivities represent the resistance to ion flow in solution and the permittivity determines the dielectric strength of the material. The elements of the model are then generated. Using small elements will result in a more accurate solution but will also increase the total number of elements, which slows the solution time and may conflict with the software limit on the number of elements. Because of this, it is advantageous to use smaller elements close to the areas of interest (i.e., the electrode site) and larger elements near the border of the model, where accuracy is less important. Finally, the boundary conditions are set. The disk electrode is set to a nonzero potential. All other surfaces are set to zero current, zero potential, or infinite ground conditions.

For given boundary conditions and material properties, COSMOS/EM approximates the potential and electric field strength for each element. It should be noted that current flow will not be determined directly by this model, since the material is not actually conducting electrons. Rather, ionic current flow will be calculated from the electric field strength at points in the volume. Figure 10 is a three-dimensional model of a probe stimulating in a bipolar configuration. The probe shank is perpendicular to the plot and the disk is in the middle of the shank. A virtual electrode exists to the left of the plot, but due to the symmetry described above, only one pole was modeled. Therefore, this is a model of shank-to-shank stimulation. This particular model is not quantitative for several reasons: the dimensions are not exactly those of the stimulating probe, the material properties of CSF are not included in the model, and the element size is not very fine near the electrode. However, several qualitative observations can be made. As expected, electric field strength is greatest near the edge of the electrode, a result that has been shown analytically. Also, the presence of the opposite pole attracts current in the direction of that pole, making the electric field stronger on one side. Current does appear to be flowing underneath the shank however. Also, near the edge of the shank, the electric field becomes concentrated. These last two phenomena could presumably be modified by the width of the shank and the placement of the electrode on the shank (currently the site is not centered in most probe designs).

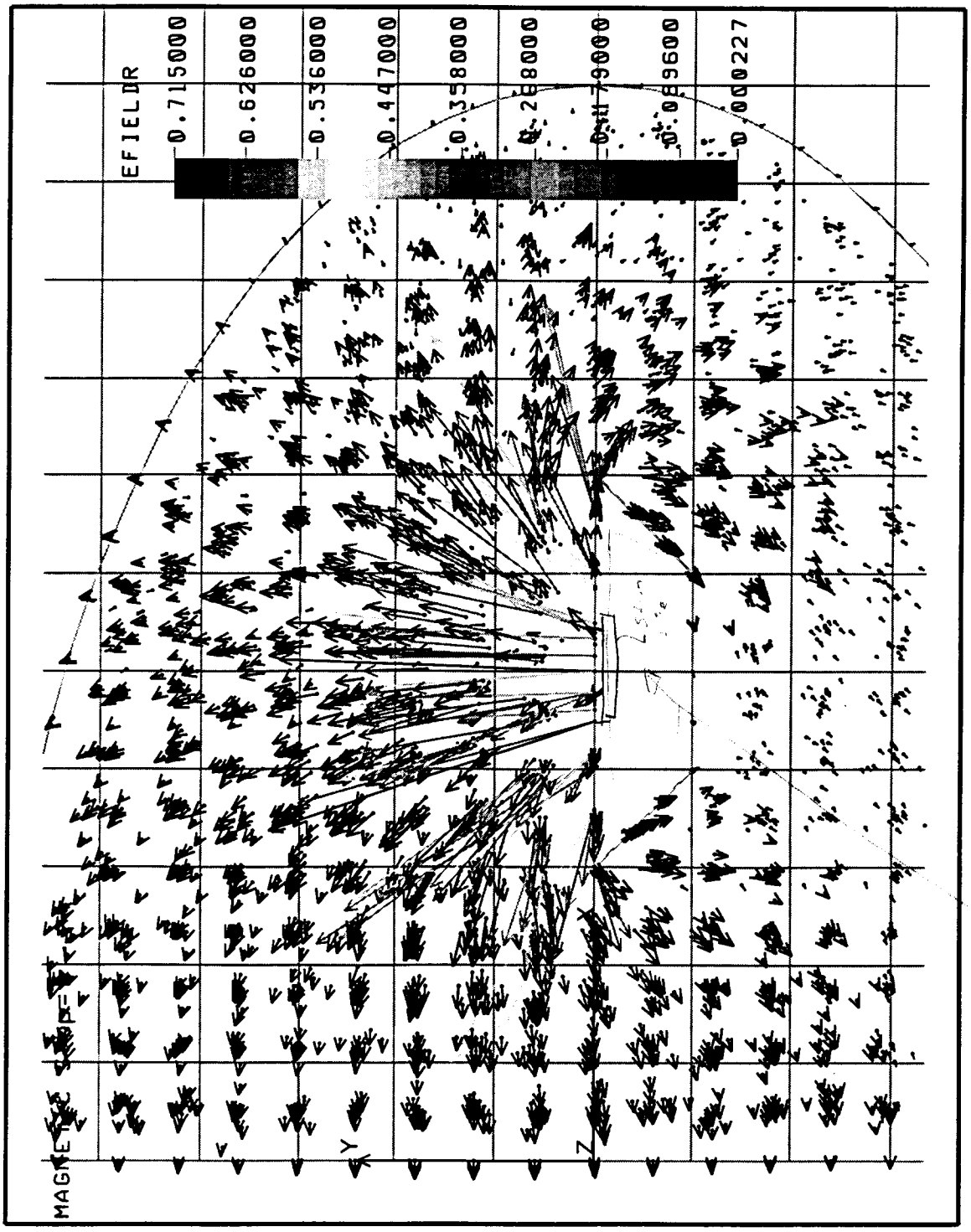


Fig. 10: Finite-element solution of the electric field around a stimulating site during bipolar stimulation. The probe shank is perpendicular to the plot and the site is in the middle of the shank. A virtual electrode exists to the left of the plot, which thus models shank-to-shank stimulation.

From these models, we hope to understand the relationships between probe geometry and tissue resistance between sites. Device design parameters that affect the resistance include the site size, site-to-site spacing, site shape, and shank width to site size ratio. We hope to create a family of curves, for both monopolar and bipolar stimulation, that relate the above variables to access resistance. Modeling will also identify areas on an electrode that can expect to experience high current densities and therefore be more susceptible to oxide corrosion or more likely to cause tissue damage.

*Analysis of Electrode Site Materials*

In the last two quarterly reports, results were presented that showed the growth of a substance on electrode sites that had been used for stimulation. The chronic experiment involved *in vivo* stimulation for five days. The probe was retrieved when the animal was sacrificed. Recently, analysis was performed on one of these electrodes using an electron microscope (Electroscan E3) to elucidate the chemical composition of the material on the site. This work was done at the University of Michigan's Electron Microbeam Analysis Laboratory. Briefly, the measurement process records the intensity of x-rays emitted when a material is bombarded with electrons. Analysis of the x-rays will produce an energy spectrum which is compared with the known spectra of various elements. The spectrum of the substance on the electrode site included peaks corresponding to carbon and oxygen, along with expected components such as silicon, iridium, and titanium. The oxygen peak may be due to the presence of iridium oxide, but the presence of carbon is still unaccounted for. One possible source, as mentioned in previous reports, would be biological material that adhered to (and perhaps overgrew) the stimulated site. One experiment cannot give us any conclusive results, but this method looks to be very useful in the future analysis of probes retrieved from chronic preparations.

*Operating Point Analysis of Activated Sites*

The electronic instrumentation used in chronic stimulation experiments was modified to allow more flexibility . A circuit was added to allow a voltage bias to be placed on the electrode site. It has been noted in previous reports and elsewhere that placing an anodic bias on an electrode will reduce its access resistance and better utilize its charge storage capacity. This circuit will allow the user to monitor the current flowing to the electrode when the bias is applied. This current should be transient. Additionally, instrumentation has been added that will allow for monopolar stimulation and recording (of the voltage drop between the electrode and ground). Previously, we had only recorded the bipolar voltage drop. That data did not allow for delineation of the several potential drops in the current loop formed by the two sites and the tissue. Recording monopolarly will provide information about the individual sites. Shortly, instrumentation will be available to do *in vivo* CV tests to evaluate the oxide during the course of a chronic experiment. Information from these long-term experiments will help define the functionality needed in active probe circuitry.

*Future Studies*

In the next quarter we hope to begin running *in vitro* stimulation experiments. These tests have been on hold until electrodes fabricated with the new metal process were available. *In vitro* testing will look at the long-term effects of pulsing and biasing on iridium oxide. Also, spectral analysis will be performed on these sites before and after testing. More models will be developed. Instrumentation should be completed that will allow us to resume *in vivo* experiments during the summer.

## *4. A Software-Controlled Site Activation Station*

Work has continued on an automated test station to grow anodically formed iridium oxide films (AIROFs) on the stimulating sites of multielectrode probe arrays. This test station is needed because the present system is outdated. In addition, this station will provide more flexibility than the present system by allowing multiple sites to be processed without continual user interaction. This will allow up to sixteen sites on a multielectrode probe array to be activated overnight. The station is capable of performing electrode site activation, cleaning, and cyclic voltammetry (CV). A block diagram of the station is shown in Fig. 11.

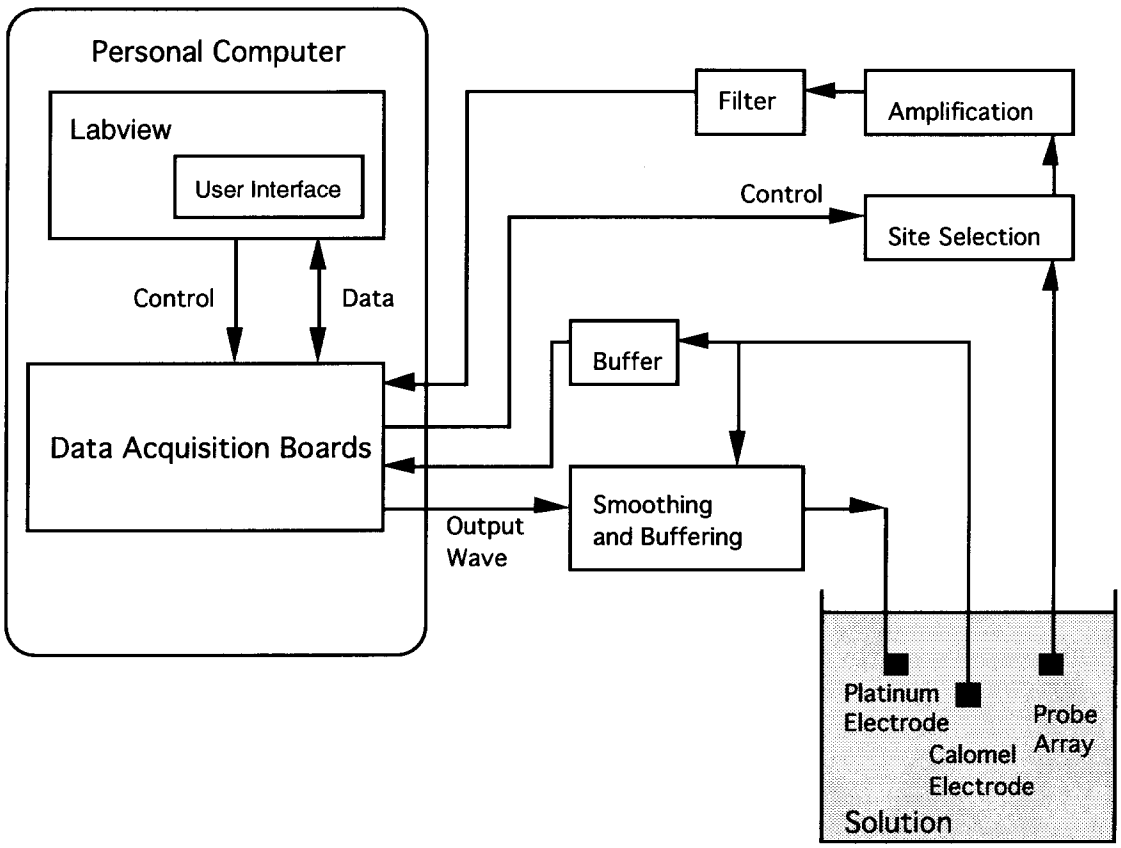


Fig. 11: Block diagram showing the new test station that is capable of activating multiple sites without continual user interaction.

Last quarter a method to more accurately measure and calculate the charge capacity was designed and implemented. The charge capacity is used to determine when activation should cease and this data for each channel is provided to the user after each CV test. The system is now operating as a laboratory tool for cleaning and activating electrodes and providing current-voltage graphs of CV tests. An example of a CV graph generated by the system is shown below in Fig. 12.

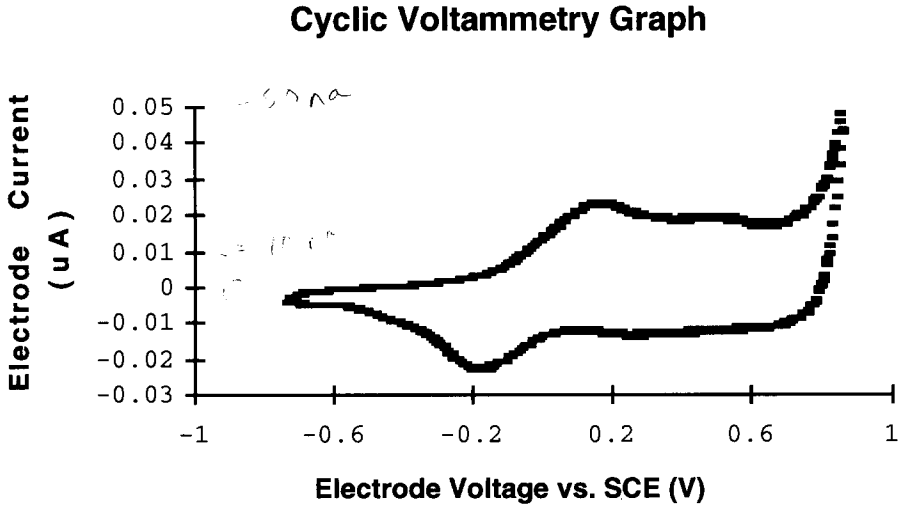


Fig. 2: Cyclic voltammetry graph generated early in the activation cycle on the new station. Site size: 1000μm$^2$.

Next quarter, the development of this new station will continue by making the final refinements in the design of the activation circuit. Further testing is required to determine a more optimal solution. Documentation for the station will be written and a method for packaging the electronics in a permanent housing must be selected and implemented.

## *5. Development of Active Stimulating Probes*

As reported in the previous quarterly report, a run of active stimulation probes was completed and is now undergoing in-vitro tests in preparation for in-vivo tests, hopefully during the coming quarter. Each of the active probes appears fully functional. During the past term, tests have been successfully conducted with the external computer interface for this probe. In addition, we have explored the current waveforms delivered by the STIM-2 probe.

STIM-2 can deliver a biphasic stimulating current over the range from 0 to ±126μA with a current resolution of about ±1μA. As set from a 16b word, a selected site can be left open between pulses (zero current) or can be shorted to ground. With a 32b word, the site can be connected to an anodic bias source between pulses. While the leakage current in the offstate has not been previously measured for these probes, it has been assumed that this leakage should be in the range of a few picoamperes, since it is composed only of reverse diode current from the output drains of the p- and n-channel output drive transistors. Using STIM-2, we bonded to an output channel and used this channel to drive a discrete 3.5nF capacitor (equivalent to a site size of about 1000μm$^2$). The voltage across the capacitor was monitored using a JFET-input opamp operated in the non-inverting unity-gain mode. The typical input current of this opamp is about 50pA. With no shunting resistor across this capacitor and the opamp connected along with STIM-2 (with the drive-current set to zero), the capacitor charged to the negative supply rail with a time constant of about 300msec, corresponding to an input current of

about 25nA. We would expect much less current than this and are trying to identify the source of the additional leakage. It appears to be due to leakage across the n-channel output sink transistors on STIM-2, and problems of insufficient sink current have been noted on some of the STIM-2 circuits. This current is still orders of magnitude less than what would be physiologically significant. When STIM-2 was used to drive the discrete capacitor with a 32μA current, the capacitor current ramped toward the supply rail with a slope of about 8.9V/msec. This is shown in Fig. 13. The drive current is also monitored across a small series resistance and was constant over a broad range in output voltage.

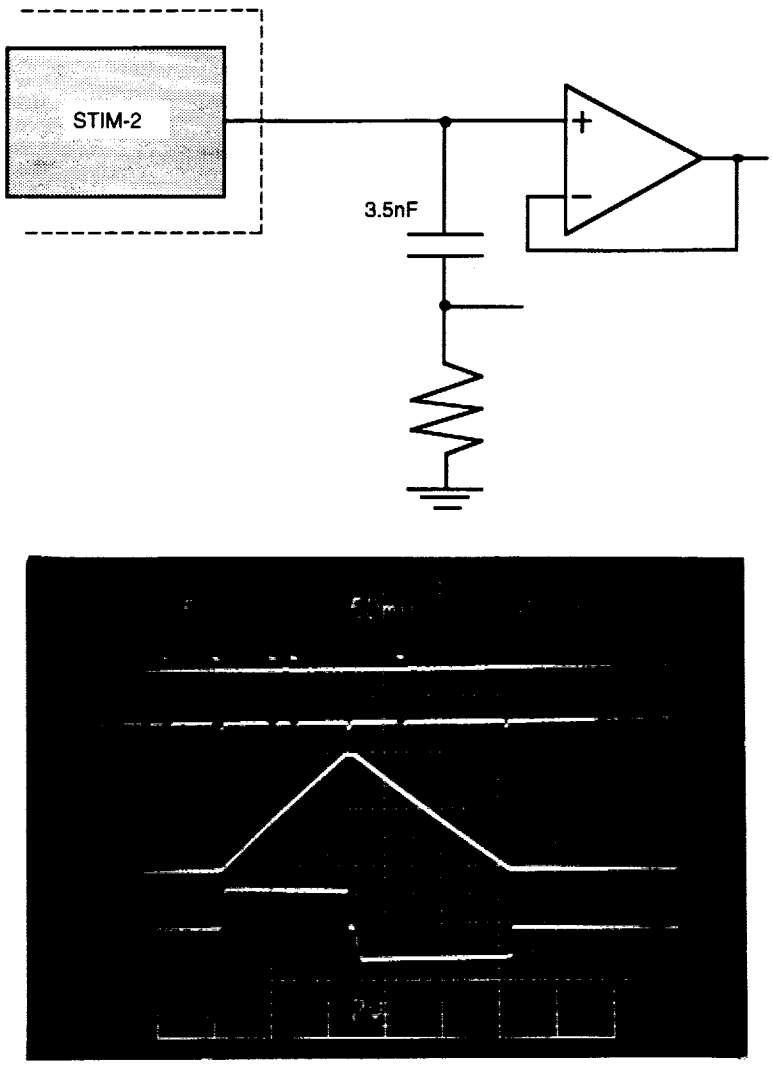


Fig. 13: Test circuit used for examining the output current from STIM-2 into a discrete capacitor. The capacitor voltage response to a 32μA current is shown in the picture below. The current is monitored across a series resistor (1kΩ) in the bottom trace, while the capacitor voltage is shown in the third trace.

The output drive circuits on STIM-2 are based on current mirrors that should keep the source and sink currents during charge-balanced stimulation balanced to within better than 1μA. Nonetheless, there will inevitably be some imbalance, and when driving an

ideal capacitor, it would be mandatory to ground the capacitor (or tie it to some other reference voltage) between pulses in order to prevent the dc capacitor voltage from "walking up" to the supply rail during repetitive pulse trains. If this caused the dc electrode voltage to exceed the water window, gassing might occur. At a low level, it is not clear that this would be physiologically harmful but it should nonetheless be avoided. If biased at the edge of the window, applied current pulses could certainly cause gassing at a significant level. Thus, grounding (or otherwise biasing) the electrode between pulses would be mandatory.

In a real iridium electrode in saline or CSF, however, the situation is somewhat different than with a real capacitor because the double layer at the electrode surface is not an ideal capacitor. Rather, it is leaky because of current flow across the double layer. Thus, the electrode will recover somewhat between pulses. In order to observe this with STIM-2 and a real electrode, a passive probe having a site area of 2000$\mu m^2$ was driven from STIM-2 using a 100$\mu$sec 10$\mu$A monophasic current pulse (intentionally charge imbalanced). Figure 14 shows the electrode voltage recovery. The electrode dc voltage is about -700mVwith respect to a Pt reference and appears to be generated by the presence of STIM-2. This might be due to the presence of the dc current noted above, which pulls the site toward the negative edge of the water window. When driven anodic first as shown, we drive away from the window edge and the electrode voltage recovers with a time constant of about 3msec. When the pulse rate was increased to 300pps (a 3.5msec interpulse interval), the electrode dc potential began noticeably "walking up" toward zero as might be expected. If the electrode was driven cathodic first, the potential waveform was reduced in amplitude and the recovery was much faster, probably indicating that the window was being exceeded. Although the recovery time is fast compared to the expected minimum interpulse interval of 5msec in normal use, this experiment appears to illustrate that if there is significant output current leakage from the drive electronics, such electrodes can be pulled to the edge of the water window where actively applied pulses can then exceed the window. Thus, although it is charge that stimulates tissue, it is essential to know the potential at which we begin electrode pulsing. It therefore appears that electrodes must be tied to a known potential between pulses. The use of anodic bias between pulses should help guard against any encroachment of the water window due to slow site charge-up in addition to providing higher charge delivery capabilities and, perhaps, greater freedom from tissue encapsulation. We are continuing to explore these aspects of electrode use to make sure the performance of these sites is thoroughly understood. The ability to bias STIM-2 sites at ground or an anodic bias between pulses will be very useful during these studies.

During the coming term, we hope to etch out additional STIM-2 probes and proceed to testing these probes in-vivo as part of the complete system.

## *6. External Electronics for Active Stimulation Probes*

The external support for stimulating probes consists of a three-component hardware system plus software. The hardware system consists of an off-the-shelf DSP processor card (Chimera) that resides in an IBM PC compatible computer. On the card itself, a custom wire-wrap circuit daughterboard translates user commands into data and clock serial pulses with the appropriate timing required by the stimulating probe. This data is transmitted over a cable to the third hardware component, a remote converter circuit, which translates the binary-valued clock and data values into the ternary-valued signals (+5, -5, and 0 volts) required by the probe.

The external hardware system features a maximum clock speed of 4 MHz but can operate in a slow mode at 0.4 MHz and is also able to generate single clock pulses for bit-by-bit testing. A high-speed FIFO on the daughterboard provides buffering for the DSP card allowing for precise timing control without the usual overhead of a real-time system. The remote converter circuitry features signal and power isolation to protect the probe and the implant subject.

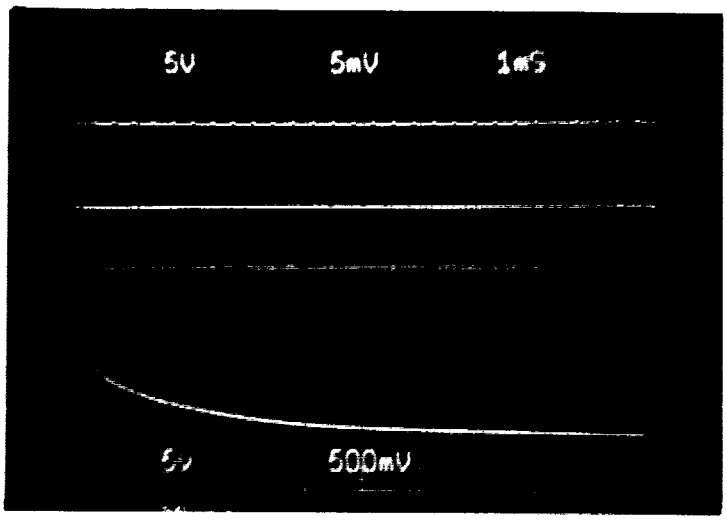


Fig. 14: Response of an activated iridium electrode having a site area of 2000$\mu m^2$ to a monopolar drive current having an amplitude of 10$\mu$A and a duration of 100$\mu$sec.

Over the last year, the design for both the daughterboard and the remote converter components was finalized and implemented. The system was tested with both STIM-1a and STIM-1b versions of the probes, and recently successfully completed integration testing with a STIM-2 probe. A software package for the IBM PC was written to support rapid prototyping and testing. The software includes a scripting language in support of repeatable and automated testing.

Work on the external stimulation support system will now shift to developing a graphical user interface for the IBM PC. This interface will incorporate the scripting language of the current text-only software but will also present a more user-friendly interface. Also, some support software must be written for the DSP processor card to allow for arbitrary real-time waveform generation.

## *7. Conclusions*

During the past quarter, research under this program has focused in several areas. We have continued to produce a variety of passive stimulating probes and provide them to internal and external users. Probes have now been fabricated using procedures reported in the last report (RTA after iridium deposition, buffered HF etch after RIE, and complete sample drying prior to sputtering) to improve iridium adhesion. Using 500Å of titanium under 3000Å of iridium with these procedures, no adhesion problems have been

observed. In addition, the interfacial barrier to current flow frequently observed in the past on metal-polysilicon contacts (electrode sites) are no longer present. We have also redefined our site formation procedure to allow thorough cleaning of the sites after RIE and before metal deposition. The new procedure uses an additional mask so that the dielectric etch and metal deposition are separate steps. Probes are now in process using this new structure. Work is also proceeding to complete the development of new site activation and characterization facilities. In addition, we are continuing modeling activities to understand current flow around implanted stimulating sites and are analyzing the material seen on stimulating sites that have been used chronically in tissue using XPS.

Active probes have now been tested successfully with the external computer interface developed for them. In addition, tests are being conducted to better understand electrode site performance when used with STIM-2. An unexpected leakage current between the sites and the negative supply rail has been noted on at least some of the STIM-2 chips. The amplitude of this current is approximately 25nA. While small, it appears that this current can polarize small electrode sites sufficiently to drag them down near the edge of the water window so that active cathodic-first stimulation would exceed the window. While studies of these phenomena are continuing, it appears that it will be necessary to tie electrodes to a known potential between pulses. This can be done with the circuitry built into STIM-2 and is in line with recent studies by other investigators that indicate such anodic bias is helpful in terms of chronic impedance and charge delivery.